First-Principles Study of K and Cs Adsorbed on Pd(111)

Wenzhen Lai and Daiqian Xie*

Institute of Theoretical and Computational Chemistry, Key Laboratory of Mesoscopic Chemistry, School of Chemistry and Chemical Engineering, Nanjing University, Nanjing 210093, China

Received: May 7, 2006; In Final Form: September 20, 2006

The adsorptions of K and Cs on Pd(111) were studied by the density functional calculations within the generalized gradient approximation. The site preference, bonding character, work function, and electron structure of the system were analyzed. For K and Cs adsorption, the hcp hollow site was found to be preferred for all the coverages investigated. The calculated adsorption geometries for (2 × 2) and ($\sqrt{3} \times \sqrt{3}$)*R*30° phases are both in reasonable agreement with the observed results. The decrease of the work function upon the adsorption of K and Cs can be attributed to a dipole moment associated with the polarized adsorbate atom, which is characterized by depletion of the electron charge in the alkali metal layer and a charge accumulation in the interface region. Our results indicate that the bonding of alkali metal with the Pd(111) surface has a mixed ionic and metallic bond character at low coverage and a metallic bond of covalent character at high coverage.

1. Introduction

Alkali metals (AM) can be used as efficient promoters in a variety of heterogeneous reactions such as the dissociations of CO, NO, N_2, and O_2,[1−3] oxidation of CO,[4,5] and Fischer−Tropsch synthesis.[6] Thus, the understanding of the chemisorption bond of AM on surface can provide important information relevant to these chemical reactions and catalytic effects on surfaces.

Considerable efforts have been devoted to investigate the AM adsorption on transition metal surfaces during the past 70 years. Experimentally, numerous techniques such as surface extended-X-ray absorption fine structure (SEXAFS),[7,8] surface core-level shift spectroscopy (SCLS),[9] photoelectron diffraction (PED),[10] low-energy electron diffraction (LEED),[11,12] and photoelectron emission microscopy (PEEM)[13] have been used to investigate the structure and diffusion of AM on the metal surfaces. The adsorption site was usually the highest coordination hollow site, while the top adsorption sites were observed on some hexagonal-symmetry substrates. In addition, substitutional-site adsorption, a result of intermixing of AM with the substrate, was found to occur for AM on Al(111), Al(100), Cu(110), and Ag(111).[11,14] The change of adsorption site with coverage was observed for three substrates, Ru(0001),[15−17] Ag(111),[18] and Rh(111).[19] For example, in the case of Cs/Ru(0001), the adsorption site changes from the top site in the p(2×2) phase to the hcp site in the ($\sqrt{3} \times \sqrt{3}$)*R*30° phase.

There are some reviews of studies for AM on metal surfaces.[20−22] In the early 1930s, Langmuir[23] and Gurney[24] developed a model (LG model) for the AM adsorption. They predicted a partial charge transfer from the AM to the substrate at very low coverages and the depolarization of these adatoms due to their mutual interactions as the coverage is increased. They also predicted a change from an ionic bond at low coverage to a nonionic bond at monolayer saturation. Later, the classical picture has been extended to the point of assuming the ionic and neutral adsorbed species coexisting on the surface.[25,26] However, the LG model was challenged in the 1980s. Both experimental[9] and theoretical studies[27,28] indicated that there is little or no charge transfer from AM to the substrate. The interaction with the substrate is described as metallic. More recently, periodic DFT calculations with a slab model have become a powerful approach to studying the adsorption of AM on the metal surfaces. Some calculations[29,30] supported that partial charge has transferred from AM to metallic substrate, while other studies[27,31] suggested that AM has a metallic bond of covalent character. In addition, combined ionic and metallic bonding was proposed to describe the K adsorption on the metal surfaces.[3]

LEED analyses have been used to study the K and Cs adsorptions in the p(2×2) and ($\sqrt{3} \times \sqrt{3}$)*R*30° phases on Pd(111).[12] It was suggested that AM−substrate bonding is of charge-transfer type by analyzing AM−substrate bond strengths. Photoelectron emission microscopy (PEEM) was also employed to study the diffusion of K on Pd(111).[32] The work function and diffusion coefficient were determined as functions of the coverage. In this work, we present a first-principles density functional study of K and Cs adsorbed on Pd(111) for coverages ranging from 0.11 to 0.33 monolayer (ML). Coverages of 0.25 and 0.33 ML [(2×2) and ($\sqrt{3} \times \sqrt{3}$) phases] were emphasized because the calculated results could be compared with experiment.[32] The saturation coverage was found to be 0.33 ML corresponding to 0.33 K atoms per substrate atom. To understand the adsorbate−substrate interaction, (2×3) and (3×3) phases, corresponding to 0.17 and 0.11 ML, were also investigated. The adsorption geometries, surface electronic structure, and adsorbate-induced work function changes were obtained and used to analyze the properties of the adsorbates.

2. Computational Details

The theoretical calculations were performed with the Vienna ab initio Simulation Package (VASP).[33,34] The electron−ion interaction is described by the projector augmented wave (PAW) method,[35,36] which is a frozen core all-electron method and believed to be good in the description of transition metals. The PAW pseudopotentials were used for all the component atoms.

* To whom correspondence should be addressed. Phone: 86-25-83596383. Fax: 86-25-83686553. E-mail: dqxie@nju.edu.cn.

10.1021/jp062788z CCC: $33.50
Published on Web 11/09/2006

TABLE 1: Adsorption Energies (eV) of K on Pd(111) at 0.33 ML[a]

parameters[b]	hcp	fcc	bridge	top
five layers; V7; 5×5×1; 350 eV	2.190	2.182 (8)	2.181 (9)	2.150 (40)
five layers; V7; 7×7×1; 350 eV	2.219	2.209 (10)	2.210 (9)	2.176 (43)
five layers; V9; 5×5×1; 350 eV	2.169	2.155 (14)	2.158 (11)	2.129 (40)
six layers; V7; 5×5×1; 350 eV	2.184	2.172 (12)	2.175 (9)	2.146 (38)
six layers; V7; 7×7×1; 350 eV	2.218	2.207 (11)	2.209 (9)	2.175 (43)
five layers; V7; 5×5×1; 400 eV	2.189	2.180 (9)	2.180 (9)	2.149 (40)
five layers; V7; 7×7×1; 400 eV	2.229	2.218 (11)	2.219 (10)	2.187 (42)

[a] Values in parentheses are the energy difference with the hcp hollow site. [b] The parameters are slab thickness, vacuum layer, *k*-points, and cutoff energy.

TABLE 2: Adsorption Energies and Geometries of K on Pd(111) with the (2 × 2) phase

site	E_{ads} (eV)	d_{K-Pd1} (Å)	l_{K-Pd1} (Å)	d_{12} (Å)	lateral (Å)	$\delta 1$ (Å)	$\delta 2$ (Å)	$\delta 3$ (Å)
without substrate rumpling, without lateral relaxation								
hcp	2.327	2.639	3.097	2.292	0	0	0	0
fcc	2.324	2.639	3.097	2.292	0	0	0	0
bridge	2.315	2.643	2.993	2.292	0	0	0	0
top	2.232	2.757	2.757	2.292	0	0	0	0
with substrate rumpling, without lateral relaxation								
hcp	2.343	2.678	3.130	2.276	0	0.087	0.003	0.003
fcc	2.338	2.672	3.125	2.273	0	0.081	0.025	0.002
bridge	2.334	2.696	3.039	2.244	0	0.094	0.002	0.002
top	2.287	2.824	2.824	2.362	0	0.166	0	0
with substrate rumpling, with lateral relaxation								
hcp	2.348	2.648	3.113	2.277	0.015	0.093	0.007	0.003
fcc	2.342	2.659	3.123	2.274	0.019	0.093	0.034	0.009
bridge	2.330	2.680	3.034	2.236	0.017	0.110	0.035	0.013
top	2.293	2.799	2.799	2.374	0.003	0.206	0.057	0.015
exp(hcp)		2.64	3.10	2.26	0.02	0.06		

The generalized gradient approximation (GGA) of Perdew and Wang (PW91)[37] was employed to deal with the electron−electron exchange-correlation energies.

We used a slab model with a five-layer slab of palladium, separated by a vacuum equivalent to seven ideal bulk palladium layers (16 Å), which is large enough to avoid the interactions between the slab and its periodic images. Four different high-symmetry adsorption sites, fcc and hcp hollow site, bridge and top site, were considered. Adsorption energies for AM (K or Cs) were computed by the following equation,

$$E_{ads} = E_{Pd(111)} + E_{AM} - E_{AM/Pd(111)} \quad (1)$$

where $E_{Pd(111)}$, E_{AM}, and $E_{AM/Pd(111)}$ are the total energies of the clean Pd(111) slab, the free AM atom, and AM on Pd(111), respectively. The relaxation of the adsorbate and substrates was performed in three different ways. In the first way, AM was allowed to relax and the total slab was fixed at the ideal bulk-terminated position. In the second way, AM and the outmost three Pd layers were allowed to relax in the vertical direction only. In the third way, AM and the outmost three Pd layers were allowed to fully relax.

The calculations of bulk properties were performed to verify the validity of the PAW pseudopotential used in this study. For bulk calculations, the energy cutoff was set to be 350 eV for the plane-wave expansion and the Brillouin zone integration was performed on a Monkhorst-Pack 15×15×15 *k*-point mesh. The pseudopotential for Pd has been generated from the reference electron configuration $4d^9 5s^1$. This resulted in a lattice constant of 3.969 Å and a bulk modulus of 156.8 GPa by using the Murnaghan equation of state. The total energy of the Pd atom required for the determination of the bulk cohesive energy was obtained by calculating a spin-polarized and nonsymmetry Pd atom in a cell of 13 Å × 14 Å × 15 Å. The calculated cohesive energy of 3.721 eV, lattice constant, and bulk modulus are in reasonable agreement with the experimental values[38] of 3.89 eV, 3.89 Å, and 180.8 GPa and previous all-electron calculated values[39] of 3.64 eV, 3.94 Å, and 163 Gpa. The generalized gradient approximation usually overestimates the lattice parameter and underestimates the bulk modulus for transition metals.[40] For the clean Pd(111) surface, no relaxation was found, which agrees well with the experimental[41] and other DFT results.[42] The pseudopotential for K and Cs treats the semicore s and p states as the valence shell. The calculated lattice constants of 5.284 Å for bulk K and 6.141 Å for bulk Cs agree reasonably with the experimental results of 5.225 and 6.045 Å,[38] respectively.

For calculations involving AM, the AM was placed on one side of the slab. Brillouin-zone integrations were performed with use of a Monkhorst-Pack[43] grid of 5×5×1 *k*-points for (2×2) and $(\sqrt{3} \times \sqrt{3})R30°$ cells. For a larger surface cell, the *k*-point grid was reduced in the corresponding direction. For (2×3) and (3 × 3) cells, we used 5×3×1 and 3×3×1 *k*-point grids, respectively. The plane wave energy cutoff was set at 350 eV. The Fermi level was smeared by the Methfessel−Paxton[44] approach with a width of 0.2 eV and the energy was corrected by extrapolation to the zero temperature.

To test the convergence of the above calculation parameters, we have performed further calculations with larger slab thickness, vacuum layer, *k*-points, and cutoff energy. The test results are summarized in Table 1. One can see from this table that, although the absolute adsorption energies from the larger parameters are within about 30 meV of the energies from the smaller parameters, the adsorption energies relative to the preferred hcp hollow site are only about several millielectronvolts. This shows that the present calculation parameters are adequate.

3. Results and Discussion

3.1. K Adsorption. *3.1.1. Adsorption Energies.* The adsorption geometries and energies for (2×2)-K and

TABLE 3: Adsorption Energies and Geometries of K on Pd(111) with the ($\sqrt{3} \times \sqrt{3}$) Phase

site	E_{ads} (eV)	d_{K-Pd1} (Å)	l_{K-Pd1} (Å)	d_{12} (Å)	lateral (Å)	δ1 (Å)	δ2 (Å)	δ3 (Å)
without substrate rumpling, without lateral relaxation								
hcp	2.176	2.641	3.096	2.292	0	0	0	0
fcc	2.170	2.641	3.101	2.292	0	0	0	0
bridge	2.160	2.644	3.013	2.292	0	0	0	0
top	2.078	2.795	2.795	2.292	0	0	0	0
with substrate rumpling, without lateral relaxation								
hcp	2.177	2.645	3.102	2.294	0	0	0.001	0
fcc	2.170	2.645	3.102	2.295	0	0	0	0
bridge	2.174	2.699	3.042	2.306	0	0.071	0	0
top	2.137	2.831	2.831	2.318	0	0.193	0	0
with substrate rumpling, with lateral relaxation								
hcp	2.190	2.638	3.111	2.289	0.019	0	0.029	0
fcc	2.182	2.664	3.128	2.302	0.030	0	0	0.002
bridge	2.181	2.676	3.034	2.268	0.028	0.086	0.015	0.003
top	2.150	2.833	2.833	2.315	0	0.241	0	0
exp(hcp)		2.64	3.10	2.27	0.03			

($\sqrt{3} \times \sqrt{3}$)*R*30°-K at four high-symmetry sites of the Pd(111) surface are listed in Tables 2 and 3, respectively. It was found that the most stable site for the K adatom is the hcp hollow site with the adsorption energy of 2.348 eV at 0.25 ML and 2.190 eV at 0.33 ML. The preference for the hcp hollow site is consistent with the experiment.[12] The adsorption energies in the fcc hollow and bridge sites are only a few millielectronvolts lower than the hcp site. The top site is the least energetically favored. The potential energy surface was found to be flat. Similar behavior has been found for K/Rh(111),[30] K/Al(111),[45] and K/Ag(111).[29] In addition, it was found that the calculated adsorption energies become lower with growing K coverage. To obtain a qualitative understanding of the relative importance of the adsorbate−adsorbate (ad−ad) and the adsorbate−substrate (ad−sub) interactions, the adsorption process could be divided into two steps: (1) K (g) → K layer ($E_1 = -\Delta E_{\text{formation of layer}}$) and (2) K layer + Pd(111) slab → K/Pd(111) ($E_2 = -\Delta E_{adh}$), where $\Delta E_{\text{formation of layer}}$ is the required energy when an isolated overlayer is produced from the isolated metal atoms. The calculated results show that $\Delta E_{\text{formation of layer}}$ increases from 0.469 eV for the (2×2) phase to 0.607 eV for the ($\sqrt{3} \times \sqrt{3}$)*R*30° phase, whereas ΔE_{adh} decreases from 1.879 to 1.583 eV. It is clear that the ad−sub interaction is more important than the ad−ad interaction.

Besides, calculations without lateral relaxation and without substrate rumpling were performed. After comparing the adsorption energies with and without substrate rumpling, it was noted that the rumpling is most important for the top site in which the energy gained by rumpling is about 60 meV, which is consistent with the finding of other AM adsorption on the metallic surfaces.[29,30] However, it is still not large enough to make the top site the preferred adsorption site. Considering the lateral displacement in the top Pd layer, it was found that only small energy is gained for all adsorption sites, which indicates that the lateral relaxation plays a minor role for the binding energy.

3.1.2. Geometries. The calculated structural parameters of the (2×2)-K and ($\sqrt{3} \times \sqrt{3}$)*R*30°-K are also presented in Tables 2 and 3. The chemisorption bond length for the AM adsorption was found to depend on their coordination to the substrate. It is shortest for the top site, longer for the bridge site, and longest for the 3-fold hollow site. The main effect of the surface rumpling is to push the atom(s) (three atoms in the case of the hollow sites, two in the bridge site, and one in the top site) under the potassium adatom deeper into the substrate, whereas the other atom(s) move outward toward the potassium layer, similar to Na/Cu(111)[31] and K/Ag(111).[29]

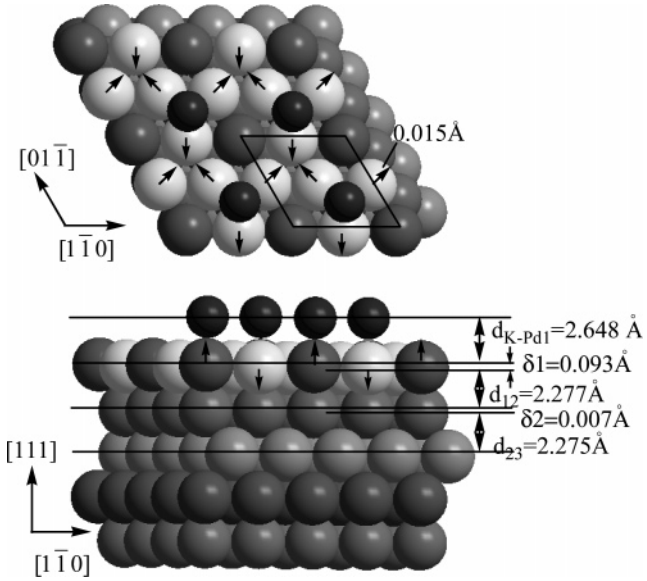

Figure 1. Top and side views of the atomic geometry of the K(2×2)/Pd(111) structure. The arrows indicate the direction of the displacements of the substrate atoms with respect to the ideal bulk positions. Small, dark gray circles represent K atoms; large white and gray circles represent Pd atoms; those lying in the same plane and are equivalent under the 3-fold symmetry are the same color. The arrows indicate the direction of the displacements of the substrate atoms with respect to the ideal bulk positions.

The optimal geometries for the hcp site in the (2×2)-K and ($\sqrt{3} \times \sqrt{3}$)*R*30°-K phases are shown in Figures 1 and 2, respectively. For the (2×2)-K phase, the vertical distance between the K layer and the top Pd layer (d_{K-Pd1}) of 2.648 Å and the corresponding K−Pd bond length of 3.113 Å agree well with the experimental values[12] of 2.64 and 3.10 Å, respectively. The lateral displacement of the atoms in the top layer was found to be 0.015 Å, which also agrees well with the experimental value of 0.02 Å. The calculated interlayer distance (d_{12}) between the first and second layers of 2.277 Å is in good agreement with the experimental value of 2.26 Å. The calculated value of 0.093 Å for surface rumpling in the first substrate layer corresponds to the experimental value of 0.06 Å. And the vertical rumpling in the second substrate layer is small (0.007 Å).

For the ($\sqrt{3} \times \sqrt{3}$)*R*30° phase, the interlayer distance d_{K-Pd1} and the corresponding K−Pd bond length were found to be 2.638 and 3.111 Å, which are very close to the values of 0.25 ML and in excellent agreement with the observed results[12]

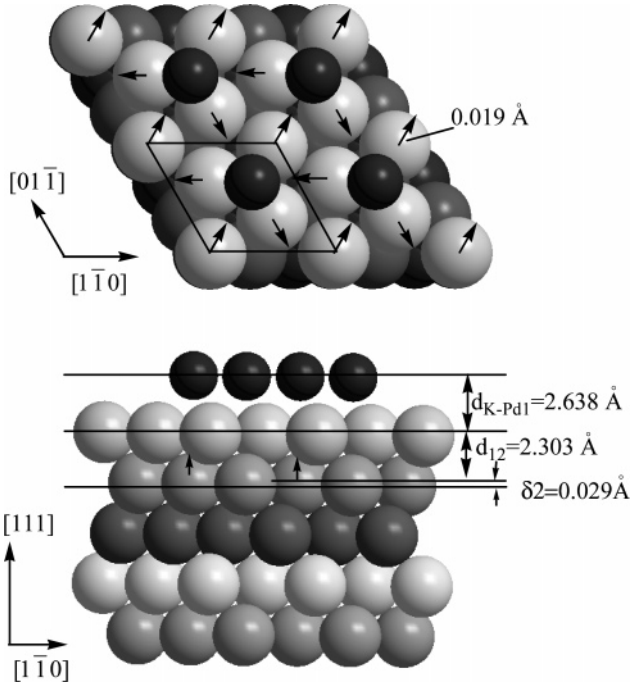

Figure 2. Top and side views of the atomic geometry of the K($\sqrt{3} \times \sqrt{3}$)/Pd(111) structure. The arrows indicate the direction of the displacements of the substrate atoms with respect to the ideal bulk positions. Small, dark gray circles represent K atoms; large white and gray circles represent Pd atoms; those lying in the same plane and are equivalent under the 3-fold symmetry are the same color. The arrows indicate the direction of the displacements of the substrate atoms with respect to the ideal bulk positions.

of 2.64 and 3.10 Å, respectively. The effective K radius, obtained from the difference of bond length and effective Pd radius ($3.97/\sqrt{8}$) is about 1.71 Å, which is about midway between the ionic (1.33 Å) and the covalent Pauling radii (2.03 Å). There is no rumpling in the first layer, due to symmetry restriction for the hollow sites in the ($\sqrt{3} \times \sqrt{3}$)*R*30° phase. Our calculations show a small relaxation of the top substrate layers. The calculated distance between the first and second Pd layers of 2.289 Å agrees well with the experimental value of 2.27 Å. In the second substrate, no rumpling is allowed for the fcc site, whereas a small rumpling of 0.03 Å was found for the hcp site, similar to the case of AM on Ag(111).[11,18]

3.1.3. Work Function. The work function was calculated as the difference between the vacuum level and the Fermi energy. The calculated value of the work function for the clean Pd(111) surface is 5.239 eV, which is slightly lower than the experimental value of 5.6 eV[46] but agrees well with other GGA calculations.[39] For AM/Pd(111), only the preferred hcp hollow site is considered for the work function calculation. After adsorption of K, the work function is reduced to 1.694 eV at 0.25 ML and 1.985 eV at 0.33 ML, which are very close to the measured values of about 1.7 eV at 0.25 ML and 2.0 eV at 0.33 ML[32] and slightly smaller than the value of 2.29 eV[46] for the polycrystalline K surface. The work function reductions of 3.545 eV at 0.25 ML and 3.254 eV at 0.33 ML were found to follow the Helmholtz equation:[39]

$$\Delta\Phi = 12\pi\theta\mu/A \qquad (2)$$

where μ is the dipole moment, A is the area of the (1×1) surface unit cell, and θ is the coverage. The calculated dipole moment per K adsorbate of 1.767 D at 0.33 ML is reduced by about 30% with respect to the result of 2.563 D at 0.25 ML. Therefore, the change of the work function can be attributed to the change of the dipole moment associated with the polarized adsorbate atom.

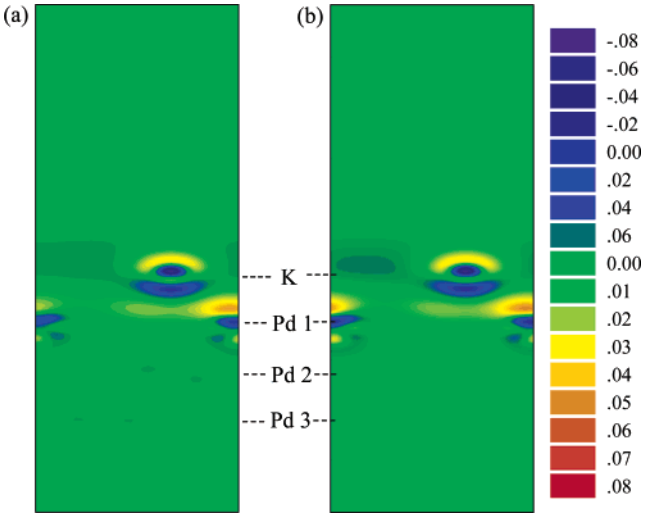

Figure 3. Difference electron density plot for K adsorbed on Pd(111) at the hcp hollow site for (a) (2×2) and (b) ($\sqrt{3} \times \sqrt{3}$)*R*30° structures. The contour plot depicts the [11$\bar{2}$] plane perpendicular to the substrate surface. The contour lines are drawn at 0.02 electrons/Å^3 intervals. The unit of both axes is Å.

3.1.4. Electronic Structure. To visualize the overall modifications of the electron distribution due to the K adsorption, the difference electron densities was evaluated as

$$\Delta\rho = \rho_{K/Pd(111)} - \rho_{Pd(111)} - \rho_K \qquad (3)$$

where $\rho_{K/Pd(111)}$, $\rho_{Pd(111)}$, and ρ_K are the electron densities for K/Pd(111), the slab, and an isolated K layer, respectively. The atomic positions of the slab and the K layer were taken to be the same as those of the relaxed K/Pd(111) system. For (2×2) and ($\sqrt{3} \times \sqrt{3}$)*R*30° phases, the difference electron densities in a plane perpendicular to the surface are shown in Figure 3. The major difference in the induced densities is the polarization of the valence electrons of K which result in a depletion of the electronic charge outside the K layer and an increase of the electronic charge in the interface region. A little charge was depleted around the fcc hollow site due to screening between the K-dipoles.

To better quantify the tendencies of the electron transfer, we have integrated the differential electron densities over planes parallel to the surface, defined as follows,

$$\Delta\rho(z) = \int \Delta\rho(x,y,z)\, dx\, dy \qquad (4)$$

Figure 4 presents the results obtained for the two phases. For the (2×2) phase, a charge depletion is visible in the vacuum region of 2−6 Å above the surface. The largest change is concentrated in the interface region (between the K adlayer and the topmost Pd layer). In addition, the charge depletes below the surface atoms. For the ($\sqrt{3} \times \sqrt{3}$)*R*30° phase, a maximum of the integrated differential density can be seen at about 1.1 Å above the surface, which is significantly lower than the maximum for the (2×2) phase. The smaller charge accumulation for the ($\sqrt{3} \times \sqrt{3}$)*R*30° phase can be attributed to the work function change, which implies a smaller interaction between the K and Pd atoms and thus a tiny charge redistribution. There is a charge depletion at about 0.4 Å above the surface for the ($\sqrt{3} \times \sqrt{3}$)*R*30° phase, while there is an accumulation for the

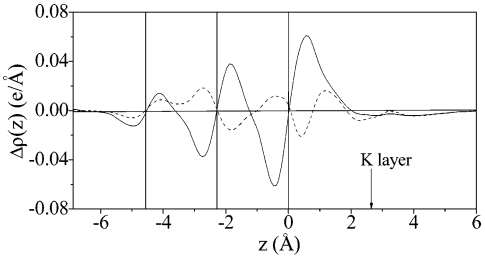

Figure 4. Difference electron density integrated for a plane parallel to the surface for K at the hcp hollow site for (2×2) [solid line] and $(\sqrt{3} \times \sqrt{3})R30°$ [dished line] structures. The average location of each of the top three Pd layers is indicated by the solid lines.

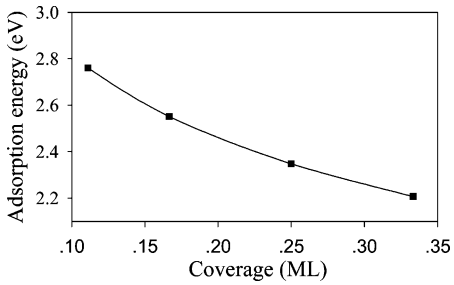

Figure 5. Adsorption energy versus coverage for K adsorption on Pd(111) at the hcp hollow sites.

(2×2) phase. It reveals that the negative charge distribution at higher coverage moves further outside from the substrate edge, indicating a metallic bonding. Therefore, it is evident that K on Pd(111) has a metallic bond of covalent character.

3.1.5. Low K Coverage. To further study the adsorbate−substrate interaction at low coverages, (2×3) and (3×3) phases were also investigated. The most stable site for both phases is also the hcp hollow site. The calculated K−Pd bond length of 3.134 for the 0.17 ML and 3.177 Å for the 0.11 ML is slightly larger than the bond length at higher coverages. Figure 5 summarizes the calculated results for the adsorption energies for K on Pd(111). It is clear that the adsorption energy decreases as the increase of the coverage. In studying K on Pt(111), Moré et al.[47] proposed that, comparing with the K adsorption energy at low coverage, the cohesive energy of K (0.9 eV) is so small that it cannot induce a condensed phase, which is also applicable for the K/Pd(111) system.

The calculated difference electron density for the (2×3) phase was found to be similar to the results at higher coverage, whereas the difference electron density for the (3×3) phase shows a significantly different behavior (see Figure 6a). The charge redistribution results in a charge depletion outside the K nuclei (4s electrons, about 2 Å from the center of K) and an increase of electronic charge in the interface region. In addition, it was found that the charge density is polarized toward the surface near the nuclei of the K atom. Thus, the K adatom is partially positive charged. It reveals that K adsorption on Pd(111) at low coverage possesses both ionic and metallic bonding properties, consistent with the picture described by Wimmer et al.[27] and Liu et al.[3]

3.2. Cs Adsorption. *3.2.1. Adsorption Energies.* The chemisorption energies for (2×2)-Cs and $(\sqrt{3} \times \sqrt{3})R30°$-Cs at the four high-symmetry sites on the Pd(111) surface are shown in Tables 4 and 5, respectively. It was found that the most stable site for the Cs adatom is also the hcp hollow site, which is consistent with experiment.[12] The adsorption energy of the adsorbed Cs decreases from 2.455 eV at 0.25 ML to 2.226 eV at 0.33 ML for the hcp hollow site. The calculated $\Delta E_{\text{formation of layer}}$ is 0.495 eV for the (2×2) phase and 0.426 eV

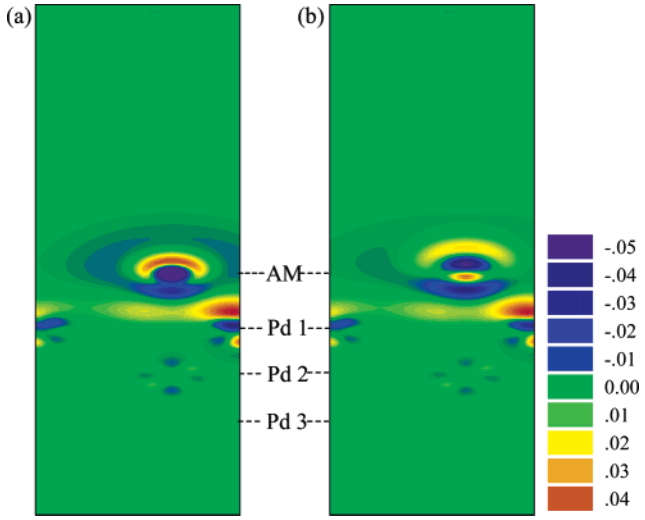

Figure 6. Difference electron density plot for (a) Pd(111)-(3×3)-K in the hcp hollow and (b) Pd(111)-(3×3)-Cs in the hcp hollow. The densities are in units of electrons/Å^3. The unit of both axes is Å.

for the $(\sqrt{3} \times \sqrt{3})R30°$ phase. Accordingly, ΔE_{adh} decreases from 1.960 to 1.800 eV with increasing coverage. It is clear that the ad−sub interaction is more important than the ad−ad interaction. The effect of the surface relaxation on the adsorption energy is similar to those observed for the K adsorption. It is worth noting that the adsorption energy for Cs adsorbed on Pd(111) is higher than that of K adsorption, whereas Moré et al.[48] suggested that the interaction with the Pt substrate for Na is larger than that for K.

3.2.2. Geometries. The calculated structural parameters of (2×2)-Cs and $(\sqrt{3} \times \sqrt{3})R30°$-Cs are also presented in Tables 4 and 5. For the (2×2)-Cs phase, the lateral displacement of the atoms in the top layer was found to be 0.015 Å, corresponding to the experimental value of 0.04 Å. The interlayer distance d_{12} of 2.295 Å, the interlayer distance $d_{\text{Cs−Pd1}}$ of 2.828 Å, and a surface rumpling of 0.057 Å are in good agreement with the corresponding experimental values of 2.26, 2.74, and 0.04 Å. For the $(\sqrt{3} \times \sqrt{3})R30°$-Cs phase, the interlayer distance d_{12} of 2.303 Å and the interlayer distance $d_{\text{Cs−Pd1}}$ of 2.797 Å agree well with the experimental values of 2.29 and 2.73 Å. There is almost no change in the Cs−Pd bond length with the coverage increasing from 0.25 to 0.33 ML. The effective Cs radius, obtained from the difference of bond length and the effective Pd radius ($3.97/\sqrt{8}$) is about 1.84 Å, which is close to the ionic Pauling radii (1.69 Å).

3.2.3. Work Function. Upon Cs adsorption, the work function is reduced to 1.608 eV at 0.25 ML and 1.753 eV at 0.33 ML, which are smaller than the work function of 1.95 eV[46] for the polycrystalline Cs surface. The calculated dipole moment is 2.629 and 1.893 D for 0.25 and 0.33 ML, respectively. It is clear that the dipole moment of Cs decreases along with the increase of the coverage. The changes of work function of 3.631 eV at 0.25 ML and 3.486 eV at 0.33 ML were found to follow the relationship given by the Helmholtz equation. This means that the surface dipole layer lowers the work function. In addition, the difference in the change of the work function between 0.25 and 0.33 ML is smaller than that of K.

3.2.4. Electronic Structure. For (2×2) and $(\sqrt{3} \times \sqrt{3})R30°$ phases, the difference electron density in a plane perpendicular to the surface is shown in Figure 7. The change in charge density is essentially localized on the first layer of the Pd atoms and the Cs atom. The Cs valence electrons were found to be

TABLE 4: Adsorption Energies and Geometries of Cs on Pd(111) with the (2 × 2) Phase

site	E_{ads} (eV)	d_{Cs-Pd1} (Å)	l_{Cs-Pd1} (Å)	d_{12} (Å)	lateral (Å)	$\delta 1$ (Å)	$\delta 2$ (Å)	$\delta 3$ (Å)
without substrate rumpling, without lateral relaxation								
hcp	2.441	2.852	3.281	2.292	0	0	0	0
fcc	2.434	2.852	3.281	2.292	0	0	0	0
bridge	2.433	2.852	3.179	2.292	0	0	0	0
top	2.396	2.859	2.859	2.292	0	0	0	0
with substrate rumpling, without lateral relaxation								
hcp	2.452	2.848	3.277	2.287	0	0.068	0.014	0.001
fcc	2.443	2.866	3.292	2.278	0	0.068	0.019	0.001
bridge	2.446	2.879	3.203	2.258	0	0.074	0.020	0.001
top	2.430	2.953	2.953	2.346	0	0.121	0.031	0.006
with substrate rumpling, with lateral relaxation								
hcp	2.455	2.828	3.267	2.295	0.015	0.057	0.010	0.001
fcc	2.446	2.854	3.289	2.274	0.014	0.075	0.025	0.009
bridge	2.448	2.874	3.206	2.253	0.017	0.082	0.022	0.010
top	2.432	2.966	2.966	2.349	0	0.129	0.033	0.009
exp(hcp)		2.74	3.17	2.26	0.04	0.04		

TABLE 5: Adsorption Energies and Geometries of Cs on Pd(111) with the ($\sqrt{3} \times \sqrt{3}$) Phase

site	E_{ads} (eV)	d_{Cs-Pd1} (Å)	l_{Cs-Pd1} (Å)	d_{12} (Å)	lateral (Å)	$\delta 1$ (Å)	$\delta 2$ (Å)	$\delta 3$ (Å)
without substrate rumpling, without lateral relaxation								
hcp	2.211	2.764	3.251	2.292	0	0	0	0
fcc	2.203	2.779	3.240	2.292	0	0	0	0
bridge	2.201	2.779	3.144	2.292	0	0	0	0
top	2.165	2.859	2.859	2.292	0	0	0	0
with substrate rumpling, without lateral relaxation								
hcp	2.218	2.818	3.251	2.306	0	0	0.001	0
fcc	2.209	2.833	3.264	2.308	0	0	0	0
bridge	2.212	2.840	3.167	2.285	0	0.059	0.002	0.002
top	2.204	2.938	2.938	2.365	0	0.149	0	0
with substrate rumpling, with lateral relaxation								
hcp	2.226	2.797	3.245	2.303	0.025	0	0.010	0
fcc	2.214	2.799	3.243	2.303	0.018	0	0	0.001
bridge	2.217	2.825	3.165	2.287	0.025	0.064	0.019	0.001
top	2.209	2.948	2.948	2.314	0	0.170	0	0
exp(hcp)		2.73	3.19	2.29	0.02			

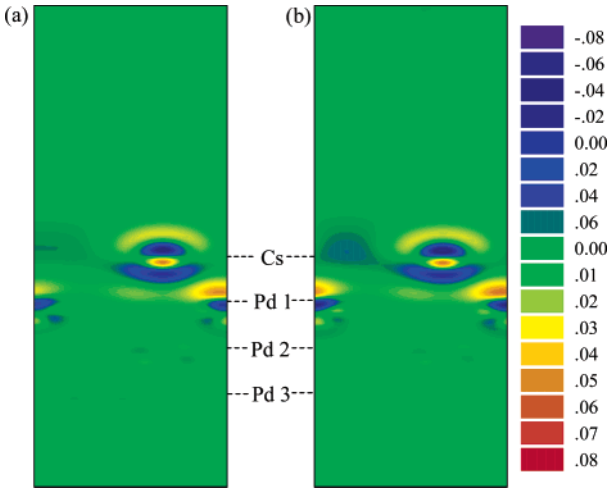

Figure 7. Difference electron density plot for Cs adsorbed on Pd(111) at the hcp hollow sites for the (a) (2×2) and (b) ($\sqrt{3} \times \sqrt{3}$)*R*30° structures. The contour plot depicts the [11$\bar{2}$] plane perpendicular to the (111) surface. Contour lines are drawn at 0.02 electrons/Å^3 intervals. The unit of both axes is Å.

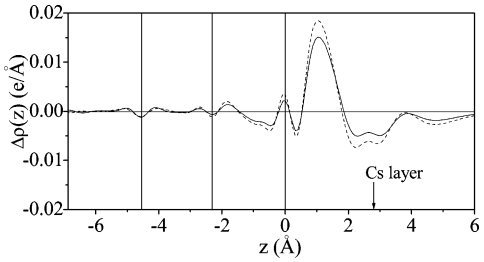

Figure 8. Difference electron density integrated for a plane parallel to the surface for Cs at the hcp hollow site for (2×2) [solid line] and ($\sqrt{3} \times \sqrt{3}$)*R*30° [dished line] structures. The average location of each of the top three Pd layers is indicated by the solid lines.

polarized toward the Pd surface, resulting in a depletion of electronic charge outside the Cs layer and an increase of electronic charge in the interface region. The Cs semicore electrons show a polarization opposite to that of the Cs valence electrons. The topmost Pd atoms are strongly polarized and their d electrons are slightly reoriented. Figure 8 displays the difference electron density integrated for a plane parallel to the surface for the two coverages. It was shown that the charge redistribution for both phases is very similar and the charge density changes are smaller in magnitude than those induced by K. The maximum in the density of transferred electrons is located in the interface region. This charge redistribution indicates a metallic bonding of covalent character, which is similar to the case of K adsorption.

3.2.5. Low Cs Coverage. The most stable site for (2×3) and (3×3) phases was also found to be the hcp hollow site. The calculated Cs−Pd bond length of 3.313 Å for 0.17 ML and 3.379 Å for 0.11 ML is larger than that at higher coverages. The adsorption energies for Cs on Pd(111) are shown in Figure 9. It is clear that the adsorption energy decreases with increasing coverage.

The difference electron density for the (3×3) phase is displayed in Figure 6b. The charge redistribution results in a

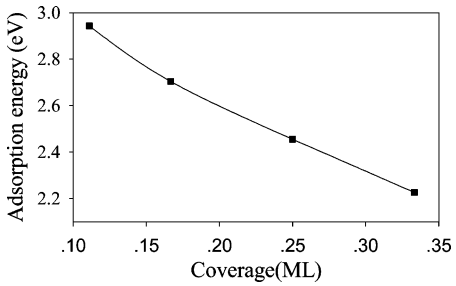

Figure 9. Adsorption energy versus coverage for Cs adsorption on Pd(111) at the hcp hollow sites.

charge depletion outside the Cs nuclei and an increase of electronic charge in the interface region. In addition, near the nuclei of the Cs atom, it was found that the charge density is polarized toward the surface. Just like K adsorption, Cs on Pd(111) at low coverage also has both ionic and metallic bonding properties.

4. Conclusion

We have studied the adsorptions of K and Cs on the Pd(111) surface. The computed geometries for both (2×2) and ($\sqrt{3} \times \sqrt{3}$)*R*30° phases are in good agreement with the experimental results. The K and Cs atoms favor to be adsorbed at the hcp sites for all coverages investigated, whereas the adsorption energy differs by only a few millielectronvolts for hcp, fcc, and bridge sites, which indicates that the potential energy surface of K or Cs on Pd(111) is flat. The rumpling and lateral displacements of Pd atoms were found to play minor roles for AM adsorption. Besides, the adsorption energies decrease with growing AM coverages, while the chemisorption bond length changes very little with the coverage.

On the other hand, our results show that the K and Cs adsorption on Pd(111) causes a significant work function decrease, which can be attributed to the dipole moment associated with the polarized adsorbate atom that is characterized by depletion of electron charge in the AM layer and a charge accumulation in the interface region. The bonding of AM with the Pd(111) surface is found to have a mixed ionic and metallic bond character at low coverages and a metallic bond of covalent character at high coverages.

Acknowledgment. This work was supported by the National Natural Science Foundation of China (Grant No.20533060).

References and Notes

(1) Whitman, L. J.; Ho, W. *J. Chem. Phys.* **1988**, *89*, 7621.
(2) Mortensen, J. J.; Hammer, B.; Norskov, J. K. *Phys. Rev. Lett.* **1998**, *80*, 4333.
(3) Liu, Z.-P.; Hu, P. *J. Am. Chem. Soc.* **2001**, *123*, 12596.
(4) Cupolillo, A.; Chiarello, G.; Formoso, V.; Pacile, D.; Papagno, M.; Veltri, F.; Colavita, E.; Papagno, L. *Phys. Rev. B* **2002**, *66*, 233407.
(5) Pacile, D.; Cupolillo, A.; Giallombardo, C.; Papagno, M.; Papagno, L. *Chem. Phys. Lett.* **2005**, *413*, 420.
(6) Somorjai, G. A. *Introduction to Surface Chemistry and Catalysis*; Wiley: New York, 1994.
(7) Lamble, G. M.; Brooks, R. S.; King, D. A.; Norman, D. *Phys. Rev. Lett.* **1988**, *61*, 1112.
(8) Schmalz, A.; Aminpirooz, S.; Becker, L.; Haase, J.; Neugebauer, J.; Scheffler, M. *Phys. Rev. Lett.* **1991**, *67*, 2163.
(9) Riffe, D. M.; Wertheim, G. K.; Citrin, P. H. *Phys. Rev. Lett.* **1990**, *64*, 571.
(10) Christensen, S. V.; Nielsen, K. T.; Nerlov, J.; Batchelor, D. R.; Adams, D. L. *Surf. Sci.* **1995**, *339*, L919.
(11) Leatherman, G. S.; Diehl, R. D.; Kaukasoina, P.; Lindroos, M. *Phys. Rev. B* **1996**, *53*, 10254.
(12) Kim, Y. D.; Schwegmann, S.; Over, H. *Phys. Chem. Chem. Phys.* **1999**, *1*, 2001.
(13) Snabl, M.; Ondrejcek, M.; Chab, V.; Stenzel, W.; Conrad, H.; Bradshaw, A. M. *Surf. Sci.* **1996**, *352*−*354*, 546.
(14) Andersen, J. N. *Surf. Rev. Lett.* **1995**, *2*, 345.
(15) Over, H.; Bludau, H.; Skottke-Klein, M.; Ertl, G.; Moritz, W.; Campbell, C. T. *Phys. Rev. B* **1992**, *45*, 8638.
(16) Hertel, T.; Over, H.; Bludau, H.; Gierer, M.; Ertl, G. *Surf. Sci.* **1994**, *301*, 1.
(17) Hertel, T.; Over, H.; Bludau, H.; Gierer, M.; Ertl, G. *Phys. Rev. B* **1994**, *50*, 8126.
(18) Kaukasoina, P.; Lindroos, M.; Leatherman, G. S.; Diehl, R. D. *Surf. Rev. Lett.* **1997**, *4*, 1215.
(19) Schwegmann, S.; Over, H. *Surf. Sci.* **1996**, *360*, 271.
(20) Diehl, R. D.; McGrath, R. *Surf. Sci. Rep.* **1996**, *23*, 43.
(21) Diehl, R. D.; McGrath, R. *J. Phys.*: *Condens. Matter* **1997**, *9*, 951.
(22) Scheffler, M.; Stampfl, C. Theory of Adsorption on Metal Substrates. In *Handbook of Surface Science;* Horn, K., Scheffler, M., Eds.; Elsevier: Amsterdam, The Netherlands, 1999; Vol. 2.
(23) Taylor, J. B.; Langmuir, I. *Phys. Rev.* **1933**, *44*, 423.
(24) Gurney, R. W. *Phys. Rev.* **1935**, *47*, 479.
(25) Hughes, F. L.; Levinstein, H. *Phys. Rev.* **1959**, *113*, 1029.
(26) Hughes, F. L. *Phys. Rev.* **1959**, *113*, 1036.
(27) Wimmer, E.; Freeman, A. J.; Hiskes, J. R.; Karo, A. M. *Phys. Rev. B* **1983**, *28*, 3074.
(28) Ishida, H. *Phys. Rev. B* **1990**, *42*, 10899.
(29) Doll, K. *Phys. Rev. B* **2002**, *66*, 155421.
(30) Xiao, H. Y.; Xie, D. Q. *Surf. Sci.* **2004**, *553*, 13.
(31) Carlsson, J. M.; Hellsing, B. *Phys. Rev. B* **2000**, *61*, 13973.
(32) Šnábl, M.; Ondrejcek, M.; Cháb, V.; Chvoj, Z.; Stenzel, W.; Conrad, H.; Bradshaw, A. M. *J. Chem. Phys.* **1998**, *108*, 4212.
(33) Kresse, G.; Furthmüller, J. *Comput. Mater. Sci.* **1996**, *6*, 15.
(34) Kresse, G.; Furthmüuller, J. *Phys. Rev. B* **1996**, *54*, 11169.
(35) Blochl, P. E. *Phys. Rev. B* **1994**, *50*, 17953.
(36) Kresse, G.; Joubert, D. *Phys. Rev. B* **1999**, *59*, 1758.
(37) Perdew, J. P.; Chevary, J. A.; Vosko, S. H.; Jackson, K. A.; Pederson, M. R.; Singh, D. J.; Fiolhais, C. *Phys. Rev. B* **1992**, *46*, 6671.
(38) Kittel, C. *Introduction to Solid State Physics*, 7th ed.; Wiley: New York, 1996.
(39) Todorova, M.; Reuter, K.; Scheffler, M. *J. Phys. Chem. B* **2004**, *108*, 14477.
(40) Li, W. X.; Stampfl, C.; Scheffler, M. *Phys. Rev. B* **2002**, *65*, 075407.
(41) Ohtani, H.; Hove, M. A. V.; Somorjai, G. A. *Surf. Sci.* **1987**, *187*, 372.
(42) Dong, W.; Kresse, G.; Furthmuller, J.; Hafner, J. *Phys. Rev. B* **1996**, *54*, 2157.
(43) Monkhorst, H. J.; Pack, J. D. *Phys. Rev. B* **1976**, *13*, 5188.
(44) Methfessel, M.; Paxton, A. T. *Phys. Rev. B* **1989**, *40*, 3616.
(45) Neugebauer, J.; Scheffler, M. *Phys. Rev. B* **1992**, *46*, 16067.
(46) Lide, D. R. *Handbook of Chemistry and Physics*, 78th ed.; CRC Press: London, UK, 1998.
(47) Moré, S.; Berndt, W.; Bradshaw, A. M.; Stumpf, R. *Phys. Rev. B* **1998**, *57*, 9246.
(48) Moré, S.; Seitsonen, A. P.; Berndt, W.; Bradshaw, A. M. *Phys. Rev. B* **2001**, *63*, 075406.